HHS Public Access

Author manuscript

Cancer Discov. Author manuscript; available in PMC 2020 May 01.

Published in final edited form as:

Cancer Discov. 2019 November ; 9(11): 1556–1573. doi:10.1158/2159-8290.CD-19-0215.

Targeting Glioblastoma Stem Cells through Disruption of the Circadian Clock

Zhen Dong[1], **Guoxin Zhang**[1], **Meng Qu**[3], **Ryan C. Gimple**[1,2], **Qiulian Wu**[1], **Zhixin Qiu**[1], **Briana C. Prager**[1,2], **Xiuxing Wang**[1], **Leo J. Y. Kim**[1,2], **Andrew R. Morton**[2], **Deobrat Dixit**[1], **Wenchao Zhou**[4], **Haidong Huang**[4], **Bin Li**[5], **Zhe Zhu**[1], **Shideng Bao**[4], **Stephen C. Mack**[6], **Lukas Chavez**[7], **Steve A. Kay**[3], **Jeremy N. Rich**[1]

[(1)]Division of Regenerative Medicine, Department of Medicine, Moores Cancer Center and Sanford Consortium for Regenerative Medicine, University of California, San Diego, CA 92037

[(2)]Department of Pathology, Case Western Reserve University School of Medicine, Cleveland, OH 44106

[(3)]Department of Neurology, Keck School of Medicine, University of Southern California, Los Angeles, CA 90089

[(4)]Department of Cancer Biology, Center for Cancer Stem Cell Research, Lerner Research Institute, Cleveland Clinic, Cleveland, OH 44106

[(5)]Ludwig Institute for Cancer Research, La Jolla, CA 92093

[(6)]Department of Pediatrics, Baylor College of Medicine, Houston, TX 77030

[(7)]Department of Medicine, University of California, San Diego, CA 92037

Abstract

Glioblastomas are highly lethal cancers, containing self-renewing glioblastoma stem cells (GSCs). Here, we show that GSCs, differentiated glioblastoma cells (DGCs), and non-malignant brain cultures all displayed robust circadian rhythms, yet GSCs alone displayed exquisite dependence on core clock transcription factors, BMAL1 and CLOCK, for optimal cell growth. Downregulation of *BMAL1* or *CLOCK* in GSCs induced cell cycle arrest and apoptosis. Chromatin immunoprecipitation revealed BMAL1 preferentially bound at metabolic genes in GSCs,

Corresponding Authors: Jeremy N. Rich, MD, Division of Regenerative Medicine, Department of Medicine, Moores Cancer Center and Sanford Consortium for Regenerative Medicine, University of California, San Diego, CA 92037, U.S.A., Phone: +1-858-822-2703, drjeremyrich@gmail.com; Steve A. Kay, PhD, Department of Neurology, Keck School of Medicine, University of Southern California, Los Angeles, CA 90089, U.S.A., Phone: +1-213-764-7964, stevekay@usc.edu.
Co-first Authors: Z. Dong, G.X. Zhang and M. Qu contributed equally to this article.

AUTHORS CONTRIBUTIONs

Conception and design: Z. Dong, G.X. Zhang, Q. Meng, R.C. Gimple, S.A. Kay and J.N. Rich.

Development of methodology: Z. Dong, G.X. Zhang, Q. Meng, R.C. Gimple, Q.L. Wu, S.A. Kay and J.N. Rich.

Acquisition of data (provide animals, managed experiments, provided facilities and assistances): Z. Dong, G.X. Zhang, Q. Meng, R.C. Gimple, Q.L. Wu, Z.X. Qiu, B.P., L.K., X.X. Wang, D. Dixit, W.C. Zhou, H.D. Huang, Z. Zhu and S. Bao, S.A. Kay and J.N. Rich.

Analysis and interpretation of data (e.g., statistical analysis, biostatistics, computational analysis): Z. Dong, G.X. Zhang, Q. Meng, R.C. Gimple, B.C. Prager, L. J.Y. Kim, B. Li, S.C. Mack, L. Chaves, S.A. Kay and J.N. Rich.

DECLARATION OF INTERESTS

The authors declare no competing interests.

Disclosures: All authors declare no competing financial interests.

associated with differences in active chromatin regions compared to NSCs. Targeting *BMAL1* or *CLOCK* attenuated mitochondrial metabolic function and reduced expression of the tricarboxylic acid (TCA) cycle enzymes. Small molecule agonists of two independent BMAL1::CLOCK negative regulators, the Cryptochromes and REV-ERBs, downregulated stem cell factors and reduced GSC growth. Combination of Cryptochrome and REV-ERB agonists induced synergistic anti-tumor efficacy. Collectively, GSCs coopt circadian regulators beyond canonical circadian circuitry to promote stemness maintenance and metabolism, offering novel therapeutic paradigms.

Keywords

Glioblastoma; circadian clock; BMAL1; CLOCK; cancer metabolism

INTRODUCTION

Glioblastoma (World Health Organization grade IV glioma) is the most prevalent and malignant primary intrinsic brain tumor (1). Standard-of-care includes maximal surgical resection followed by chemoradiation with the oral methylator, temozolomide, then adjuvant temozolomide, which offers only palliation (2). While glioblastoma has been extensively characterized at the molecular level (3), translation of this knowledge to clinical practice has been limited.

Glioblastomas display remarkable cellular heterogeneity, contributing to high rates of therapeutic resistance and rapid recurrence (4,5). Glioblastomas contain self-renewing, tumor-initiating cells, GSCs (6–8). Although the precise identity of GSCs remains controversial due to a lack of universally informative GSC markers and functional assays, GSCs have been reliably demonstrated in glioblastoma and promote tumor angiogenesis, brain invasion, and immune evasion (9–11).

Altered circadian regulation in cancer stem cells may contribute to disease progression (12). Endogenous circadian rhythms are established by two transcription-translation negative feedback loops, in which the positive limb is composed of the basic helix-loop-helix-Per-Arnt-Sim (bHLH-PAS) transcriptional factors, BMAL1 (Brain and Muscle ARNT-Like 1; also known as Aryl hydrocarbon Receptor Nuclear Translocator-Like protein 1, ARNTL) and CLOCK (Circadian Locomotor Output Cycles Kaput), which form heterodimers (13), with the transcriptional output linked to metabolism, immune regulation, and other cellular pathways (14,15). The BMAL1::CLOCK complex drives the rhythmic expression of the negative limb proteins, PERIOD (PER1/2/3) and CRYPTOCHROME (CRY1/2), which form a complex to inhibit BMAL1-CLOCK transcriptional activity (16). The BMAL1::CLOCK complex also induces REV-ERBα and REV-ERBβ, which directly transcriptionally repress *BMAL1* expression, constituting a second feedback loop (17). In some cancers and model systems, *BMAL1* or *CLOCK* serve as oncogenes (12,18,19), but, in others, their targeting is tumor suppressive (20–22). Recent systems analysis revealed that alteration of circadian genes is correlated with patient survival and clinical outcomes in several tumor types (23). Circadian networks in glioblastoma may be oncogenic with an association between gene variants and tumor incidence, and targeting circadian regulators may reduce tumor growth

and improve efficacy of chemotherapy (24,25). Based on this background, we investigated the integrity of the core circadian circuitry within GSCs.

RESULTS

Genetic disruption of core circadian genes inhibits GSC growth

To study the circadian rhythm and core circadian genes in glioblastoma, we monitored circadian clock activity utilizing a luciferase reporter driven by the *BMAL1* promoter. Although MYC has been proposed to disrupt the normal circadian rhythm (26) and GSCs express high MYC levels (27), patient-derived GSCs and their differentiated progeny, displayed circadian rhythms with similar properties to non-malignant brain cultures derived from epilepsy surgical resections (NMs), independent of tumor genetics (Fig. 1A–D; Supplementary Fig. S1A–S1K). Consistent with the observed rhythmicity, BMAL1 bound to core clock genes, including *PER1/2, CRY1/2* and *NR1D1/2* in GSCs, as measured by BMAL1 chromatin immunoprecipitation followed by deep sequencing (ChIP-seq; Supplementary Fig. S1L–S1N). Canonical rhythms observed in normal brain cells and GSCs suggest that cellular transformation maintains circadian rhythms, despite the activation of oncogenes.

To study the functional roles of core circadian genes, *BMAL1* and *CLOCK* were targeted by shRNA-mediated knockdown in patient-derived GSCs and NMs using two non-overlapping shRNAs compared to a control non-targeting shRNA sequence (shCONT). Targeting either *BMAL1* or *CLOCK* potently impaired proliferation in GSCs derived from multiple patients (Fig. 1E–H; Supplementary Fig. S2A–S2F). In contrast, targeting *BMAL1* or *CLOCK* minimally reduced cell proliferation in epilepsy-derived brain cultures or neural stem cells (NSCs) (Fig. 1I–L; Supplementary S2G and S2H), with modest anti-proliferative effects in DGCs (Supplementary Fig. S2I–S2L). Reduced GSC proliferation upon *BMAL1* or *CLOCK* knockdown was confirmed by CRISPR/Cas9-mediated knockout (Fig. 1M–1P). As *NPAS2* partially compensates for the loss of CLOCK in some tissues (28), we measured *NPAS2* mRNA expression in different cell types; while NSCs and NMs had the lowest and highest *NPAS2* mRNA expression respectively, GSCs expressed moderate *NPAS2* mRNA levels (Supplementary Fig. S2M). A mild trend towards lower expression of NPAS2 in GSCs was observed compared to that in DGCs (Supplementary Fig. S2N). *BMAL1* or *CLOCK* knockdown in GSCs induced minimal changes in *NPAS2* expression (Supplementary Fig. S2O–S2Q). Targeting *NPAS2* moderately reduced GSC proliferation compared to *CLOCK* knockdown (Supplementary Fig. S2R–S2T). These data suggest that *NPAS2* may function in GSCs, but appears largely distinct from the role of *CLOCK*. Collectively, our results indicate that core clock regulators are required for GSC growth, likely by regulating novel biological processes rather than cell-specific modulation of the core circadian rhythm.

Targeting circadian regulators induces cell cycle arrest and apoptosis in GSCs

To determine the cellular effects of *BMAL1* and *CLOCK* knockdown in GSCs, we analyzed cell cycle progression and apoptosis upon modulation of BMAL1 and CLOCK. GSCs transduced with sh*BMAL1* or sh*CLOCK* displayed reduced G_1 and increased G_2/M fractions compared to GSCs transduced with shCONT (Fig. 2A and B). Gene Set

Enrichment Analysis (GSEA) revealed decreased expression of G_2/M and M phase genes with *BMAL1* knockdown (Fig. 2C and D). Cell proliferation rate was substantially reduced in sh*BMAL1*- and sh*CLOCK*-transduced GSCs by EdU incorporation and Ki67 staining (Fig. 2E and F; Supplementary Fig. S3A–S3F). Flow cytometric measurement of Annexin V and propidium iodide (PI) staining revealed induction of apoptosis by *BMAL1* and *CLOCK* knockdown relative to shCONT (Fig. 2G; Supplementary Fig. S3G–S3J). Cleaved CASPASE 3 was also induced upon targeting *BMAL1* or *CLOCK* (Fig. 2H; Supplementary Fig. S3K–S3N), confirmed by cleaved poly-ADP ribose polymerase (PARP) (Supplementary Fig. S3M and S3N). However, Z-VAD-FMK, a pan-CASPASE inhibitor, did not rescue the cellular death induced in GSCs after *BMAL1* or *CLOCK* knockdown, suggesting that multiple mechanisms contribute to the loss of GSC viability (Supplementary Fig. S3O and S3P). As *Cry* knockout improves chemotherapy efficacy through *p73*-mediated apoptosis by increasing *TP73* expression (29), we examined *TP73* expression in GSCs after *BMAL1* or *CLOCK* knockdown, but no difference was found (Supplementary Fig. S3Q and S3R), suggesting alternative mechanisms underlie GSC clock dependence. Collectively, these results indicated that *BMAL1* and *CLOCK* are indispensable for cell proliferation and survival of GSCs.

Disruption of circadian transcriptional circuitry impairs GSC self-renewal

To determine whether core circadian genes *BMAL1* and *CLOCK* are important for maintenance of stemness in GSCs, self-renewal was measured by limiting dilution sphere formation. Upon downregulation of *BMAL1* or *CLOCK*, both sphere formation frequency (considered a surrogate of self-renewal) and sphere size (considered a surrogate of proliferation) were reduced, revealing impairment of self-renewal (Fig. 2I–L). Disruption of *BMAL1* or *CLOCK* in GSCs decreased the expression of core GSC maintenance transcription factors, including *SOX2*, *OLIG2* and *MYC*, as measured by RT-PCR and immunoblot (Fig. 2M–P). BMAL1 bound the promoters of *SOX2*, *OLIG2* and *MYC*, measured by ChIP-seq and ChIP-qPCR (Fig. 2Q; Supplementary Fig. S3S–S3U). Thus, the circadian machinery is essential for maintaining stem cell transcriptional regulator levels and the subsequent self-renewal properties of GSCs, likely through transcriptional regulation.

The GSC epigenetic landscape reprograms circadian regulation

Circadian gene regulation is mediated through binding of the BMAL1::CLOCK heterodimeric transcriptional complex. The selective dependency of GSCs on *BMAL1* and *CLOCK* expression in cell growth and survival, relative to their normal counterpart, suggests that core clock proteins must regulate gene expression programs in GSCs distinct from those in normal stem cells. Therefore, we performed BMAL1 ChIP-seq in two GSCs and two NSCs. Unsupervised clustering of each BMAL1 ChIP-seq sample by principal component analysis (PCA) revealed that GSCs and NSCs showed divergent BMAL1 occupancy across the genome (Supplementary Fig. S4A). BMAL1 peaks were distributed across the genome with enrichment at promoter regions in GSCs compared to NSCs, consistent with greater occupancy of BMAL1 in regions surrounding transcription start sites (TSSs) genome-wide (Fig. 3A and B; Supplementary Fig. S4B). To understand the functional consequences of differential BMAL1 occupancy genome-wide, we defined BMAL1 peaks with increased occupancy in GSCs and NSCs (Supplementary Fig. S4C and S4D). Expanded BMAL1

binding site occupancy occurs despite similar *BMAL1* or *CLOCK* expression levels in GSCs relative to NSCs (Supplementary Fig. S4E and S4F). Consistent with previous studies (30), the conserved E-box motif (CACGTG) was enriched within GSC-gained BMAL1 peaks, although additional de novo motifs were revealed by motif enrichment analysis (Fig. 3C). Most BMAL1 binding genes in NSCs were shared with GSCs (87%; 7,194 genes out of 8,266 total NSC target genes). In contrast, BMAL1 target genes in GSCs were largely distinct from those in NSCs (50%; 8,507 genes out of 16,773 total GSC target genes) (Fig. 3D). This suggests that GSCs reprogram BMAL1 binding genome-wide, which in turn drives novel transcriptional function. To gain insight into the unique biological functions of BMAL1 in GSCs, we applied GSEA to identify molecular pathways selectively driven by BMAL1 occupancy in GSCs. GSEA for GSC-gained BMAL1 peaks within 3-kb of a transcription start site revealed an enrichment of pathways regulating circadian clock transcriptional networks, as expected, but also regulation of glucose metabolism and lipid biosynthesis (Fig. 3E–I; Supplementary Fig. S4G). In differentiated organs, BMAL1 targets across the genome are largely tissue-specific (31) (Supplementary Fig. S4H). Although many genes bound by BMAL1 in murine liver, kidney or heart were shared with GSC-specific BMAL1 binding sites, the large majority of GSC-specific BMAL1 sites were distinct from those seen in normal tissues (Supplementary Fig. S4I–S4L). These results suggest that the majority of BMAL1 binding sites gained in GSCs (6683 of 8508, 78.5%) are distinct from sites in tissues in which BMAL1 is known to regulate metabolism. Taken together, these data suggest that BMAL1 gains unique functions in GSCs beyond generation of circadian oscillations and that this core circadian regulator has been repurposed to regulate tumor metabolism in GSCs.

We next aimed to characterize the epigenomic features responsible for the differential binding of BMAL1 between GSCs and NSCs, based on the hypothesis that BMAL1 binds novel binding sites in GSCs due to differential access to chromatin in GSCs and NSCs. Histone H3 lysine 27 acetylation (H3K27ac) ChIP-seq was performed on GSCs and NSCs to define active chromatin regions. Overlapping the BMAL1 and H3K27ac ChIP-seq revealed that BMAL1 signals strongly correlated with H3K27ac signals (Fig. 3J). Almost all GSC-gained BMAL1 peaks (11,338 of 12,386 peaks; 92%) overlapped with H3K27ac peaks, which defined active promoter/enhancer regions (Fig. 3K). Further, chromatin regions with GSC-gained BMAL1 peaks presented higher H3K27ac signals in GSCs compared to NSCs (Supplementary Fig. S4M). Chromatin regions with GSC-gained BMAL1 peaks containing E-box motifs exhibited higher H3K27ac signals in GSCs compared to NSCs (Supplementary Fig. S4N). Collectively, these data suggest that the distinct patterns of BMAL1 binding in GSCs and NSCs may be influenced by differential chromatin activity surrounding selected E-box motifs in GSCs. This model predicts stronger overlapping between GSC-gained H3K27ac peaks and BMAL1 binding in GSCs than in NSCs. To test this, we analyzed BMAL1 binding around chromatin regions enriched with GSC-gained H3K27ac peaks and found that BMAL1 signals were much higher at those regions in GSCs compared to NSCs (Supplementary Fig. S4O). BMAL1 binds to multiple gained E-box motifs at the promoter regions of genes in various tissues and cells, so we examined BMAL1 binding around chromatin regions containing E-box and enriched with GSC-gained H3K27ac. Consistent with the hypothesis, BMAL1 signals are much higher in GSCs around the chromatin regions

having E-box and GSC-gained H3K27ac marks compared to those in NSCs (Fig. 3L). Combined analysis of H3K4me3 ChIP-seq, BMAL1 ChIP-seq and H3K27ac ChIP-seq data revealed that the majority of gained BMAL1 peaks (11381 of 12386 peaks; 91.9%) in GSCs overlapped with H3K4me3 peaks (Fig. 3M). Most of the overlapped peaks (8441 of 11381 peaks; 74.2%) from BMAL1 ChIP-seq and H3K4me3 ChIP-seq overlapped with H3K27ac peaks (Supplementary Fig. S4P). The strongest BMAL1 signals were found at the active TSSs marked by H3K4me3 (Fig. 3N). In contrast, few BMAL1 peaks (305 of 12386 peaks; 2.5%) were found at enhancer regions marked by H3K27ac alone (Supplementary Fig. S4P). These data indicate preferential binding of BMAL1 at active TSSs in GSCs.

In summary, BMAL1 occupancy is distinct between GSCs and NSCs, with preferential binding defined by the underlying differences in chromatin activity between GSCs and NSCs. Interrogating the differential targets of BMAL1 between GSCs and NSCs revealed that BMAL1 may gain novel functions in GSCs to support aberrant tumor metabolism. The greater genome-wide binding of BMAL1 in GSCs than NSCs mirrored the greater distribution of active chromatin, as marked by H3K27ac, suggesting that differences in downstream BMAL1 transcriptional regulation is derived, at least in part, from the greater accessibility of binding sites in GSCs (Fig. 3O).

BMAL1 and CLOCK maintain metabolic homeostasis in GSCs

Core circadian genes regulate multiple metabolic processes, including glucose and lipid metabolism, oxidative phosphorylation, and mitochondrial dynamics (32,33). BMAL1 ChIP-seq showed that GSC-gained BMAL1 binding occupies about half of metabolic genes analyzed (Supplementary Fig. S5A). Targeting *BMAL1* reduced the expression of most selectively BMAL1-bound metabolic genes in GSCs, as revealed by RNA-seq data (Supplementary Fig. S5B). To better understand the biological functions of BMAL1 and CLOCK in GSCs, we derived gene sets from GSC-gained BMAL1 binding, revealing enrichment of glucose metabolism (Fig. 3E–I; Supplementary Fig. S4G). Individual genes, including prominently cancer-related metabolic genes, demonstrated increased BMAL1 and H3K27ac binding in GSCs compared to NSCs (Supplementary Fig. S5C–S5K).

Based on the association of BMAL1 with metabolic genes, we interrogated BMAL1 and CLOCK regulation of bioenergetics through glycolysis and the tricarboxylic acid (TCA) cycle in GSCs. Glycolysis and oxidative phosphorylation (OXPHOS) were monitored using an extracellular flux analyzer (XF) by measuring oxygen consumption rate (OCR) and extracellular acidification rate (ECAR) after *BMAL1* or *CLOCK* knockdown. OCR was inhibited in two patient-derived GSCs upon knockdown of either *BMAL1* or *CLOCK* (Fig. 4A and B). Decreased mitochondrial respiration was reflected in reduced basal OCR (Fig. 4C and D), ATP-capacity (Fig. 4E and F), and uncoupled OCR upon targeting *BMAL1* or *CLOCK* (Fig. 4G and H). Further, *BMAL1*- or *CLOCK*-deficient GSCs showed significant reduction in ECAR, indicating decreased glycolysis (Supplementary Fig. S6A and S6B). Basal glycolysis after glucose treatment in *BMAL1* or *CLOCK* shRNA-transduced GSCs was similar to control shCONT. Targeting *BMAL1* or *CLOCK* followed by oligomycin-induced stressed glycolysis exhibited greater decrease compared with basal level

(Supplementary Fig. S6C and S6D). Thus, the circadian regulators BMAL1 and CLOCK promote mitochondrial OXPHOS and glycolysis in GSCs.

OXPHOS and glycolysis involve many different metabolic enzymes. BMAL1 ChIP-seq (Supplementary Fig. S5C–S5K) and ChIP-qPCR (Fig. 4I and J) indicate that BMAL1::CLOCK heterodimers may directly regulate OXPHOS and glycolysis in GSCs by binding to the promoters of glycolysis genes (*HK2* and *LDHA*) and TCA cycle genes (*ACO2*, *IDH3A*, *SDHA* and *CS*). This notion is supported by reduced transcription of these genes upon *BMAL1* or *CLOCK* knockdown (Fig. 4K; Supplementary Fig. S6E–S6H). Metabolites generated by the TCA cycle were measured by mass spectrometry, revealing reduction in the levels of succinate, isocitrate, malate and fumarate compared with other metabolites, such as pyruvate, in GSCs following knockdown of *BMAL1* or *CLOCK* (Supplementary Fig. S6I–S6K). Collectively, BMAL1 and CLOCK control essential metabolic activity, in part, by directly regulating the expression of genes important for glycolysis and the TCA cycle in GSCs.

Mitochondrial fission-fusion dynamics are regulated in a circadian manner through dynamin-related protein 1 (DRP1) regulation and targeting *BMAL1* induces swollen and dysfunctional mitochondria (34,35). Upon *BMAL1* or *CLOCK* knock down, we detected no obvious differences in protein levels of DRP1 and PINK1 (PTEN-induced kinase 1), nor phosphorylated DRP1 in GSCs (data not shown), suggesting that BMAL1 and CLOCK control the OXPHOS independent from mitochondrial dynamics.

Succinate dehydrogenase is controlled by BMAL1 and CLOCK and essential for GSC maintenance

To extend the understanding of circadian control of GSC metabolism, we interrogated enzymes that have been linked to tumor growth and were specifically downregulated in GSCs upon targeting *BMAL1* or *CLOCK*. Succinate dehydrogenase (SDHA) is a unique enzyme participating in both the TCA cycle and the electron transport chain. We observed consistently decreased SDHA levels after transduction with either sh*BMAL1* or sh*CLOCK* (Supplementary Fig. S6L). *SDHA* knockdown reduced the levels of stemness markers, *SOX2* and *OLIG2* (Fig. 4L), induced apoptosis measured by cleavage of CASPASE 3 and PARP (Fig. 4M), and abolished growth of GSCs (Fig. 4N and O). Pharmacologic inhibition of SDHA using ß-nitropropionic acid (NPA) repressed GSC growth to a greater degree than either DGCs or non-malignant brain cells (Fig. 4P), suggesting that TCA disruption differentially represses GSC proliferation.

Pharmacological targeting of circadian machinery in GSCs specifically impairs GSC survival

BMAL1 and CLOCK are transcription factors, which are notoriously challenging to target, especially in the brain, where drug delivery is highly restricted. However, the circadian machinery has two, independent negative feedback loops for which pharmacologic agents have been developed as agonists or stabilizers that would be expected to disrupt the positive circadian activity mediated by BMAL1 and CLOCK. SR9011 and SR9009 are small molecule agonists of nuclear receptors REV-ERBα/β, which negatively regulate *BMAL1*

transcription by directly binding to its promoter (Fig. 5A) (36). SR9011 and SR9009 treatment reduced expression of the circadian regulators, *BMAL1, PER1* and *PER2*, in a concentration-dependent manner (Fig. 5B and C). SR9009 and SR9011 treatment attenuated the expression of GSC markers, *OLIG2* and *SOX2*, supporting negative transcriptional regulation of key GSC targets (Fig. 5D and E). SR9011 and SR9009 also reduced GSC cell proliferation to a greater degree than DGCs, astrocytes, and non-malignant brain cultures, demonstrating greater sensitivity of GSCs, as measured by EC_{50} (Fig. 5F and G). Consistent with *BMAL1* knockdown in GSCs, REV-ERBs agonists reduced the expression of genes in glycolysis, TCA cycle, and lipid metabolism (Supplementary Fig. S7A–S7F), consistent with prior observations (37).

Distinct from REV-ERBs, CRY1 and CRY2, two other core clock components, function by interacting directly with BMAL1::CLOCK complexes to repress their activity (16). KL001 (N-(3-(9H-carbazol-9-yl)-2-hydroxypropyl)-N-(furan-2-ylmethyl) methane-sulfonamide), a carbazole derivative previously discovered in our high-throughput cell-based screens, stabilizes CRYs by inhibiting FBXL3-mediated ubiquitination and degradation of CRY proteins (Fig. 5H) (38). CRYs represent attractive targets for agonism/stabilization in several disease areas such as inflammation, metabolic disease and cancers (29,39,40). Here, we found that KL001 decreased expression of *PER1* and *PER2* but increased BMAL1 protein levels, in a concentration-dependent manner in GSCs (Fig. 5I; Supplementary Fig. S7G). KL001 decreased *OLIG2* and *SOX2* expression in GSCs (Fig. 5J) and inhibited GSC proliferation more effectively than normal brain cells and DGCs (Fig. 5K). CRY1 overexpression decreased MYC levels and impaired GSC proliferation (Fig. 5L–N). Thus, pharmacological modulation of circadian components may offer a novel strategy for improving glioblastoma treatment.

Combinatorial pharmacologic REV-ERBs and CRYPTOCHROME agonists inhibit GSC growth

Targeting circadian control of GSCs through monotherapies of REV-ERB or CRY agonists selectively repress GSC growth. We hypothesized that combinatorial activation of both major negative feedback loops of the circadian rhythm could augment disruption of GSC growth. Indeed, combination of REV-ERBs and CRY agonists displayed combinatorial efficacy against two patient-derived GSCs (Fig. 6A–D; Supplementary Fig. S8A–S8D). Combinations of SR9011 and KL001 reduced cell growth in a concentration-dependent manner to a greater degree than single treatments (Fig. 6E–H). To evaluate the combination of SR9011 and KL001 on maintenance of stemness, self-renewal was measured by the limiting dilution assay. Following treatment with combined agents, sphere formation frequency (Fig. 6I and J) and sphere size (Supplementary Fig. S8E) were reduced, revealing greater impairment of self-renewal capacity than either single agent alone. Combined treatment also reduced the expression of core clock genes and the metabolic genes, indicating the on-targeting affects (Fig. 6K). Cleaved caspase 3 staining in GSCs following combined drug treatment showed a marked induction of apoptosis compared with either single agent (Fig. 6L and M; Supplementary Fig. S8F). Combined drug treatment also augmented disruption of cell cycle progression, as assessed by EdU incorporation assay and Ki67 staining (Fig. 6N and O; Supplementary Fig. S8G–S8H). Enhanced apoptosis in GSCs

after combined drug treatment was confirmed by increased cleaved-PARP (Fig. 6P). GSCs display potent cell migration, so we performed wound healing assays, revealing that the wound closure was delayed following treatment with two agonists (Fig. 6Q and R), suggesting combination of SR9011 and KL001 impaired cell migration ability in GSCs. Collectively, these results demonstrate proof-of-concept for combinatorial targeting of both negative circadian feedback loops in the disruption of GSC proliferation and survival.

Genetic and small molecules targeting of core clock components in GSCs inhibits tumor growth

To address whether disruption of core circadian genes influences in vivo brain tumor growth, we implanted GSCs transduced with either shCONT or shRNAs targeting *BMAL1* or *CLOCK* into the frontal lobes of immunocompromised mice. The lifespan of tumor-bearing mice nearly doubled upon *BMAL1* or *CLOCK* knockdown, relative to controls (Fig. 7A and B). Tumor-bearing brains harvested 20 days after GSC transplantation revealed no visible or very small tumors in mice bearing GSCs transduced with either sh*BMAL1* or sh*CLOCK*, while tumors reaching our endpoint criteria were present in mice bearing GSCs transduced with shCONT (Fig. 7C–F). To validate these loss-of-function studies, we performed reciprocal gain-of-function experiments, revealing that GSCs with BMAL1 overexpression proliferated more rapidly than GSCs expressing EGFP (Supplementary Fig. S8I and S8J). Mice bearing GSCs overexpressing BMAL1 survived for shorter periods than mice bearing GSCs transduced with EGFP (Supplementary Fig. S8K and S8L). Taken together, these results demonstrate that BMAL1 and CLOCK contribute significantly to in vivo tumor growth of GSCs.

While REV-ERB agonists have been previously tested in glioblastoma preclinical studies using mouse cells (25), CRY agonists offer a novel therapeutic route. In vivo tool molecules derived from KL001 have been developed and shown to be efficacious in preclinical models of diabetes (41). We tested one of the most promising proof-of-concept tool molecules, SHP656, to characterize potential utility of CRY stabilizers for glioblastoma therapy. Treating patient-derived GSCs, DGCs or non-malignant (NM) epilepsy-derived neural cells with different concentrations of the compound, SHP656 selectively reduced the cell number of GSCs, without obvious suppression of DGCs or NMs at the same concentrations (2–30 μM) (Figure 7G). To determine potential in vivo efficacy, we implanted GSCs bearing a luciferase reporter into the frontal lobes of mice, and treatment was initiated once measurable tumors were evident. SHP656 was well-tolerated, with no evidence of weight loss or changes in mouse behavior (Supplementary Fig. S8M and S8N). SHP656 treatment prolonged the survival of mice bearing two different patient-derived GSCs compared with non-treatment (Fig. 7H and I). Thus, targeting the circadian rhythm of GSCs via CRY stabilizing compounds to inhibit tumor growth in vivo is a viable treatment paradigm to pursue.

To determine the potential clinical utility of targeting the circadian rhythm machinery, we interrogated *BMAL1* expression in The Cancer Genome Atlas (TCGA), revealing that *BMAL1* mRNA levels were elevated in glioblastomas relative to lower grades of glioma and other glioma histologies (Fig. 7J and K). High *BMAL1* expression was associated with poor

prognosis across tumor grades and within glioblastoma (Fig. 7L and M), whereas higher levels of the circadian clock repressors, CRY2, REV-ERBα, PER2 and PER3 were associated with improved survival in glioma patients (Fig. 7N–Q). These data support targeting the BMAL1::CLOCK axis as a promising strategy for glioblastoma therapy in humans.

DISCUSSION

Disruption of circadian function in oncogenic processes has been largely considered at the systems level. Analysis of TCGA data identified correlations between tumor-types and tumor-stage specific alteration of cyclic clock genes with patient survival across 32 cancer types (23). Despite these insights for a role of circadian dysregulation in cancer, few novel mechanisms of action to guide new cancer therapies have emerged. Here, we report that cancer stem cells derived from patients afflicted with glioblastomas recruit core components of the circadian molecular machinery to regulate noncanonical target genes, distinct from those in the corresponding normal cells. GSCs exhibit unique chromatin landscapes that reprogram the output of BMAL1::CLOCK-dependent transcriptional regimes. Circadian rhythmicity was preserved in multiple patient-derived GSCs with different genetic backgrounds. Although MYC antagonizes circadian rhythms in cancer cells (26), GSCs with *MYC* amplification or high expression demonstrated robust cyclic activity of luminescence. Growth of normal brain cells and differentiated tumor cells was resistant to genetic or pharmacological disruption of circadian circuitry. In contrast, GSCs display high sensitivity to circadian targeting, with associated loss of viability and diminished self-renewal. Furthermore, gain-of-function studies in GSCs revealed that *BMAL1* expression accelerates tumor growth, providing further support for an oncogenic role for BMAL1::CLOCK activity in the cancer stem cell compartment. Our findings in fully transformed cancer cells stand in contrast to previous reports that a circadian rhythm and core clock genes function as tumor suppressors during initial tumorigenesis (20,21), suggesting that the role of core clock function in tumor progression may differ based on tumor development stage, cell type and species differences. Consistent with our observations presented here, *BMAL1* and *CLOCK* are oncogenic in myeloid leukemia stem cells (12). These findings point to a global reprogramming of circadian gene regulation, rather than the presence or absence of overt rhythms in cancer cells, as being critical for understanding how the clock can be targeted for novel therapies.

Widespread transcriptional regulation by circadian networks is reflected in the breadth of reported phenotypes connecting circadian regulators to cancer biology, including tumor metabolism, metastasis, and immune dysregulation (14,21,42). The observation that specifically targeting circadian regulators diminishes viability of GSC populations opens the possibility that modulating circadian machinery could offer novel treatment paradigms, e.g. combinations with traditional cytotoxic therapies, anti-angiogenics, or emerging immuno-oncology approaches. We recently identified GO289, a highly potent and specific inhibitor of Casein Kinase 2 that regulates PER phosphorylation and circadian gene expression (43), which suppressed *BMAL1* transcription and reduced viability in renal cell carcinoma and acute myeloid leukemia cells versus non-malignant cell lines. Mathematical modeling of radiation administration has indicated that timing of radiation treatment for glioblastoma

may also improve tumor control (44). Circadian timing of treatment affected sensitivity of glioblastoma cells to temozolomide in vitro, with maximal chemotherapy-induced DNA damage responses, activation of apoptosis, and growth inhibition occurring near the daily peak of *BMAL1* expression (24). In contrast to the traditional focus on chronotherapy being on optimal timing of treatments, we propose that the identification of the ectopic rewiring of BMAL1::CLOCK in GSCs provides the rationale to develop glioblastoma therapies with novel mechanisms of action.

The observations that GSCs express and depend on core circadian regulators could have several explanations, all of which can contribute to the development of experimental therapeutics. BMAL1 binding to cell-type specific promoters is mediated by tissue-specifically distributed histone modifications controlling transcription factor accessibilities at the TSSs of target genes which regulate output profile (45). Our analysis of BMAL1 and H3K27ac ChIP-seq in GSCs and NSCs revealed strong correlation between BMAL1 peaks, H3K27ac peaks as well as H3K4Me3 peaks. Genome-wide BMAL1 occupancy in GSCs was more extensive and showed higher peak intensity at active chromatin regions, as indicated by H3K27ac modification, compared to NSCs. BMAL1 displayed higher enrichment at E-box motifs with higher H3K27ac occupancy in GSCs, as compared with NSCs. Thus, differential BMAL1 binding between GSCs and NSCs is most likely driven by the different epigenetic states and subsequently different chromatin accessibility at target sites including stemness genes. Based on our analysis of the genome-wide binding of BMAL1 and the differential chromatin landscape of GSCs compared to NSCs, we propose that BMAL1 (and CLOCK) drives ectopic transcriptional programs via novel target binding sites, including canonical binding sites (CLOCK and BMAL1), but also conserved binding sites associated with ETS family members (ETV4 and ETV6) as well as key regulators of chromatin tertiary structure (YY1, YY2 and CTCF) (Fig. 3C). The broad net effect on transcription programs promotes key tumor metabolic effects on glucose and lipid metabolism, as well as EGFR signaling (Fig. 3F), which itself has been linked to lipid metabolism (46). Consistent with the idea that *BMAL1* and *CLOCK* drive networks that promote oncogenesis, we see specific molecular targets that are regulated by *BMAL1* in GSCs (e.g. hexokinase 2 and SDHA) that have been independently linked to tumor maintenance (47,48). The collective emergent properties of this previously unidentified reprogramming in GSCs strongly support the maintenance of tumor growth selectively in the stem-like tumor cells.

Disordered mitochondrial OXPHOS in our study, which is consistent with previous studies in other models (32), reinforced the critical roles of core clock genes in maintaining metabolic states that support tumor growth. We and others have found that glucose metabolism is critical to maintenance of GSCs, which selectively take up glucose through a high affinity uptake mechanism (49). *BMAL1* or *CLOCK* maintained GSCs by promoting glycolysis and TCA cycle, supported by the reduced glycolysis and TCA cycle accompanied by decreased levels of TCA metabolites in GSCs upon *BMAL1* or *CLOCK* knockdown (Fig. 4A–H; Supplementary Fig. S6A–S6F, S6I and S6J). Maintained pyruvate levels in GSCs after *BMAL1* or *CLOCK* knockdown may be attributed to reduced consumption of pyruvate due to reduced TCA cycling (Fig. S6K). Tumor metabolism generates oncometabolites that can serve as functional modulators or co-factors of chromatin

regulators (50,51). GSC circadian rhythms may have a feedforward effect, whereby cooption of BMAL1::CLOCK activity, aligned with the relatively open chromatin of GSCs, may promote oncogenic effects that ultimately feedback to maintain the open chromatin state. Thus, the targeting of core circadian clock machinery in GSCs may represent a topological vulnerability that results in disruption of this feedforward mechanism and collapse of cell state, that does not occur in NSCs or DGCs. Therapies that directly modulate circadian regulators may augment the efficacy of pharmacologic agents that target tumor metabolism (e.g. DCA) or chromatin states (e.g. EZH2, BMI1, or KDM inhibitors). BMAL1 and CLOCK are bHLH-PAS transcription factors, which are commonly considered as undruggable, but pharmacological modulation of the core circadian feedback loop has been undertaken through two distinct feedback mechanisms; both of which we have investigated. Here, SR9011 and SR9009 displayed high efficacy against GSCs (~2 fold more responsive then DGCs and up to ~25 fold more responsive than non-malignant cells), which is consistent with previous reports in mouse cell lines (25), although SR9009 also has REV-ERB independent effects (52). We extend the therapeutic hypothesis by demonstrating reduced stemness upon treatment, supporting the potential benefit of targeting core clock genes for cancer therapy.

Repressing BMAL1::CLOCK activity by modulating CRYs presents an entirely novel approach for glioblastoma treatment, and offers the possibility of combinatorial therapy with emerging as well as established agents. KL001 is a carbazole derivative identified in a phenotypic cell-based screen (38). KL001 results in the stabilization of CRY1 and CRY2 proteins by binding the FAD pocket subsequently reducing binding to the FBXL3 ubiquitin ligase and proteolysis (53). Here, we found that KL001 and its derivative, SHP656, are highly potent in killing GSCs compared to other cell types. Parallel to this high specificity, SHP656 has shown minor toxicity when administered to mouse (Supplementary Fig. S8M and S8N). Consistent with the known mode of action of CRY proteins (12), KL001 treatment suppressed E-Box dependent core clock gene expression such as *PER1* and *PER2*. In addition to its canonical effects, KL001 potently reduces the expression of several genes required to maintain stemness. Although preclinical derivates of KL001 and SHP656 have been developed and applied to treatment for metabolic diseases (38,41), this is their first known application in oncology.

The link between the circadian clock and aging (54), suggests that circadian control may be differentially regulated in pediatric brain tumors. Recent studies have demonstrated that pediatric brain tumors are molecularly distinct from adult brain tumors, with frequent mutations in core histone proteins (55), which induce epigenetic reprogramming, possibly altering available binding sites for BMAL1. Future studies will define circadian regulation of pediatric brain tumors and potential utility of targeting the circadian clock in these important cancers.

GSC resistance to current therapies represents a significant unmet medical need for glioblastoma patients. Targeting of one or more components of the circadian machinery offers a compelling new path for the development of novel therapies in combination with conventional therapies, radiation and chemotherapy.

METHODS

Derived Glioblastoma Stem Cells

Patients undergoing surgical resection for glioblastomas at Duke University or University Hospitals-Case Medical Center provided written informed consent in accordance with a protocol (090401) approved by Institutional Review Board (United States). All patient related studies were conducted in accordance with the Declaration of Helsinki. After review by neuropathology, excess glioblastoma surgical specimens were obtained. Validated brain tumor initiating cells were isolated from glioma specimen and xenograft through prospective sorting and functionally characterized, as previously described (56). Short Tandem Repeat (STR) analyses were performed to authenticate the identity of GSCs used in this article yearly. Mycoplasma testing was performed by PCR using cellular supernatants. To decrease the incidence of artifacts caused by in vitro culture, patient derived xenografts were propagated as a renewable source of tumor cells. Cells were grown in vitro fewer than 10 passages for *in vitro* and *in vivo* experiments.

Intracranial Tumor Formation *in vivo*

All mice procedures were performed under an animal protocol approved by University of California, San Diego Institutional Animal Care and Use Committee. Intracranial transplantation of GSCs was performed as previously described (56). Viable 50,000 cells transduced with shRNA for 48 hours were injected intracranially into the right cerebral cortex of NSG (NOD.Cg-Prkdcscid ll2rgtm1Wjl/SzJ, the Jackson Laboratory) immunocompromised mice. To compare the tumor growth, Brain were isolated from mice implanted with GSCs on the same day when there was development of neurological signs after implantation. For the survival experiment, mice were maintained until manifestation of neurological signs.

For in vivo therapy, NSG mice were implanted intracranially with 20,000 cells. After 7 days, mice were divided into a vehicle control (1% CMC) group and a SHP656 group. The reagents were administered by oral gavage (10 mg/kg BID for T387, and OD for T3565) until endpoints were reached. Identical volumes of vehicle were given to the control group.

RNA Isolation and Quantitative RT-PCR

Cellular RNA was isolated and reverse-transcribed to cDNA using cDNA synthesis kit (ABI, 4387406). Then RT-PCR was performed using SYBR Green Mastermix (ABI, 4309155) on an Applied Biosystems 7900HT cycler with primers (Table S1).

For all complete experimental details, reagents and statistical analyses, please see Supplementary Methods and Supplementary reagents.

DATA AND SOFTWARE AVAILABILITY

All newly generated raw sequencing data is available on GEO through the accession number: GSE134974. All data from external sources has been referenced in methods.

Supplementary Material

Refer to Web version on PubMed Central for supplementary material.

ACKNOWLEDGMENTS

We appreciate the UCSD Histology Core for their work on histologic experiments and analysis. We thank Kunliang Guan, Bing Ren, Mark Perelis, and Rich lab members for their help. Figure 3O was prepared in part using images from Servier Medical Art by the Servier (https://smart.servier.com/).

Financial support: The work was supported by NIH grants (CA197718, CA154130, CA169117, CA171652, NS087913, and NS089272 to J.N. Rich; DK108087 to S.A. Kay; CA184090, NS091080, NS099175 to S. Bao; CA217066 to B.C. Prager; CA217065 to R.C. Gimple; CA203101 to L.J.Y. Kim; CA236313 to A.R. Morton).

REFERENCES

1. Ostrom QT, Gittleman H, Liao P, Vecchione-Koval T, Wolinsky Y, Kruchko C, et al. CBTRUS Statistical Report: Primary brain and other central nervous system tumors diagnosed in the United States in 2010–2014. Neuro Oncol 2017;19(suppl_5):v1–v88 doi 10.1093/neuonc/nox158. [PubMed: 29117289]
2. Stupp R, Mason WP, van den Bent MJ, Weller M, Fisher B, Taphoorn MJ, et al. Radiotherapy plus concomitant and adjuvant temozolomide for glioblastoma. The New England journal of medicine 2005;352(10):987–96 doi 10.1056/NEJMoa043330. [PubMed: 15758009]
3. Brennan CW, Verhaak RG, McKenna A, Campos B, Noushmehr H, Salama SR, et al. The somatic genomic landscape of glioblastoma. Cell 2013;155(2):462–77 doi 10.1016/j.cell.2013.09.034. [PubMed: 24120142]
4. Patel AP, Tirosh I, Trombetta JJ, Shalek AK, Gillespie SM, Wakimoto H, et al. Single-cell RNA-seq highlights intratumoral heterogeneity in primary glioblastoma. Science 2014;344(6190):1396–401 doi 10.1126/science.1254257. [PubMed: 24925914]
5. Meyer M, Reimand J, Lan X, Head R, Zhu X, Kushida M, et al. Single cell-derived clonal analysis of human glioblastoma links functional and genomic heterogeneity. Proceedings of the National Academy of Sciences of the United States of America 2015;112(3):851–6 doi 10.1073/pnas.1320611111. [PubMed: 25561528]
6. Chen J, Li Y, Yu TS, McKay RM, Burns DK, Kernie SG, et al. A restricted cell population propagates glioblastoma growth after chemotherapy. Nature 2012;488(7412):522–6 doi 10.1038/nature11287. [PubMed: 22854781]
7. Singh SK, Hawkins C, Clarke ID, Squire JA, Bayani J, Hide T, et al. Identification of human brain tumour initiating cells. Nature 2004;432(7015):396–401 doi 10.1038/nature03128. [PubMed: 15549107]
8. Galli R, Binda E, Orfanelli U, Cipelletti B, Gritti A, De Vitis S, et al. Isolation and characterization of tumorigenic, stem-like neural precursors from human glioblastoma. Cancer research 2004;64(19):7011–21 doi 10.1158/0008-5472.CAN-04-1364. [PubMed: 15466194]
9. Bao S, Wu Q, Sathornsumetee S, Hao Y, Li Z, Hjelmeland AB, et al. Stem cell-like glioma cells promote tumor angiogenesis through vascular endothelial growth factor. Cancer research 2006;66(16):7843–8 doi 10.1158/0008-5472.CAN-06-1010. [PubMed: 16912155]
10. Wakimoto H, Kesari S, Farrell CJ, Curry WT Jr., Zaupa C, Aghi M, et al. Human glioblastoma-derived cancer stem cells: establishment of invasive glioma models and treatment with oncolytic herpes simplex virus vectors. Cancer research 2009;69(8):3472–81 doi 10.1158/0008-5472.CAN-08-3886. [PubMed: 19351838]
11. Zhou W, Ke SQ, Huang Z, Flavahan W, Fang X, Paul J, et al. Periostin secreted by glioblastoma stem cells recruits M2 tumour-associated macrophages and promotes malignant growth. Nature cell biology 2015;17(2):170–82 doi 10.1038/ncb3090. [PubMed: 25580734]
12. Puram RV, Kowalczyk MS, de Boer CG, Schneider RK, Miller PG, McConkey M, et al. Core Circadian Clock Genes Regulate Leukemia Stem Cells in AML. Cell 2016;165(2):303–16 doi 10.1016/j.cell.2016.03.015. [PubMed: 27058663]

13. Takahashi JS. Transcriptional architecture of the mammalian circadian clock. Nature reviews Genetics 2017;18(3):164–79 doi 10.1038/nrg.2016.150.

14. Bass J, Takahashi JS. Circadian integration of metabolism and energetics. Science 2010;330(6009): 1349–54 doi 10.1126/science.1195027. [PubMed: 21127246]

15. Cao Q, Zhao X, Bai J, Gery S, Sun H, Lin DC, et al. Circadian clock cryptochrome proteins regulate autoimmunity. Proceedings of the National Academy of Sciences of the United States of America 2017;114(47):12548–53 doi 10.1073/pnas.1619119114. [PubMed: 29109286]

16. Kume K, Zylka MJ, Sriram S, Shearman LP, Weaver DR, Jin X, et al. mCRY1 and mCRY2 are essential components of the negative limb of the circadian clock feedback loop. Cell 1999;98(2): 193–205. [PubMed: 10428031]

17. Preitner N, Damiola F, Lopez-Molina L, Zakany J, Duboule D, Albrecht U, et al. The orphan nuclear receptor REV-ERBalpha controls circadian transcription within the positive limb of the mammalian circadian oscillator. Cell 2002;110(2):251–60. [PubMed: 12150932]

18. Janich P, Pascual G, Merlos-Suarez A, Batlle E, Ripperger J, Albrecht U, et al. The circadian molecular clock creates epidermal stem cell heterogeneity. Nature 2011;480(7376):209–14 doi 10.1038/nature10649. [PubMed: 22080954]

19. Li A, Lin X, Tan X, Yin B, Han W, Zhao J, et al. Circadian gene Clock contributes to cell proliferation and migration of glioma and is directly regulated by tumor-suppressive miR-124. FEBS letters 2013;587(15):2455–60 doi 10.1016/j.febslet.2013.06.018. [PubMed: 23792158]

20. Kettner NM, Voicu H, Finegold MJ, Coarfa C, Sreekumar A, Putluri N, et al. Circadian Homeostasis of Liver Metabolism Suppresses Hepatocarcinogenesis. Cancer cell 2016;30(6):909–24 doi 10.1016/j.ccell.2016.10.007. [PubMed: 27889186]

21. Papagiannakopoulos T, Bauer MR, Davidson SM, Heimann M, Subbaraj L, Bhutkar A, et al. Circadian Rhythm Disruption Promotes Lung Tumorigenesis. Cell metabolism 2016;24(2):324–31 doi 10.1016/j.cmet.2016.07.001. [PubMed: 27476975]

22. Tang Q, Cheng B, Xie M, Chen Y, Zhao J, Zhou X, et al. Circadian Clock Gene Bmal1 Inhibits Tumorigenesis and Increases Paclitaxel Sensitivity in Tongue Squamous Cell Carcinoma. Cancer research 2017;77(2):532–44 doi 10.1158/0008-5472.CAN-16-1322. [PubMed: 27821487]

23. Ye Y, Xiang Y, Ozguc FM, Kim Y, Liu CJ, Park PK, et al. The Genomic Landscape and Pharmacogenomic Interactions of Clock Genes in Cancer Chronotherapy. Cell systems 2018;6(3): 314–28 e2 doi 10.1016/j.cels.2018.01.013. [PubMed: 29525205]

24. Slat EA, Sponagel J, Marpegan L, Simon T, Kfoury N, Kim A, et al. Cell-intrinsic, Bmal1-dependent Circadian Regulation of Temozolomide Sensitivity in Glioblastoma. Journal of biological rhythms 2017;32(2):121–9 doi 10.1177/0748730417696788. [PubMed: 28470120]

25. Sulli G, Rommel A, Wang X, Kolar MJ, Puca F, Saghatelian A, et al. Pharmacological activation of REV-ERBs is lethal in cancer and oncogene-induced senescence. Nature 2018;553(7688):351–5 doi 10.1038/nature25170. [PubMed: 29320480]

26. Altman BJ, Hsieh AL, Sengupta A, Krishnanaiah SY, Stine ZE, Walton ZE, et al. MYC Disrupts the Circadian Clock and Metabolism in Cancer Cells. Cell metabolism 2015;22(6):1009–19 doi 10.1016/j.cmet.2015.09.003. [PubMed: 26387865]

27. Wang J, Wang H, Li Z, Wu Q, Lathia JD, McLendon RE, et al. c-Myc is required for maintenance of glioma cancer stem cells. PloS one 2008;3(11):e3769 doi 10.1371/journal.pone.0003769. [PubMed: 19020659]

28. Landgraf D, Wang LL, Diemer T, Welsh DK. NPAS2 Compensates for Loss of CLOCK in Peripheral Circadian Oscillators. PLOS Genetics 2016;12(2):e1005882 doi 10.1371/journal.pgen. 1005882. [PubMed: 26895328]

29. Ozturk N, Lee JH, Gaddameedhi S, Sancar A. Loss of cryptochrome reduces cancer risk in p53 mutant mice. Proceedings of the National Academy of Sciences of the United States of America 2009;106(8):2841–6 doi 10.1073/pnas.0813028106. [PubMed: 19188586]

30. Koike N, Yoo S-H, Huang H-C, Kumar V, Lee C, Kim T-K, et al. Transcriptional Architecture and Chromatin Landscape of the Core Circadian Clock in Mammals. Science 2012;338(6105):349–54 doi 10.1126/science.1226339. [PubMed: 22936566]

31. Beytebiere JR, Trott AJ, Greenwell BJ, Osborne CA, Vitet H, Spence J, et al. Tissue-specific BMAL1 cistromes reveal that rhythmic transcription is associated with rhythmic enhancer-

enhancer interactions. Genes & development 2019;33(5–6):294–309 doi 10.1101/gad.322198.118. [PubMed: 30804225]

32. Peek CB, Affinati AH, Ramsey KM, Kuo HY, Yu W, Sena LA, et al. Circadian clock NAD+ cycle drives mitochondrial oxidative metabolism in mice. Science 2013;342(6158):1243417 doi 10.1126/science.1243417. [PubMed: 24051248]
33. Cho H, Zhao X, Hatori M, Yu RT, Barish GD, Lam MT, et al. Regulation of circadian behaviour and metabolism by REV-ERB-alpha and REV-ERB-beta. Nature 2012;485(7396):123–7 doi 10.1038/nature11048. [PubMed: 22460952]
34. Jacobi D, Liu S, Burkewitz K, Kory N, Knudsen NH, Alexander RK, et al. Hepatic Bmal1 Regulates Rhythmic Mitochondrial Dynamics and Promotes Metabolic Fitness. Cell metabolism 2015;22(4):709–20 doi 10.1016/j.cmet.2015.08.006. [PubMed: 26365180]
35. Schmitt K, Grimm A, Dallmann R, Oettinghaus B, Restelli LM, Witzig M, et al. Circadian Control of DRP1 Activity Regulates Mitochondrial Dynamics and Bioenergetics. Cell metabolism 2018;27(3):657–66 e5 doi 10.1016/j.cmet.2018.01.011. [PubMed: 29478834]
36. Solt LA, Wang Y, Banerjee S, Hughes T, Kojetin DJ, Lundasen T, et al. Regulation of circadian behaviour and metabolism by synthetic REV-ERB agonists. Nature 2012;485(7396):62–8 doi 10.1038/nature11030. [PubMed: 22460951]
37. Solt LA, Wang Y, Banerjee S, Hughes T, Kojetin DJ, Lundasen T, et al. Regulation of circadian behaviour and metabolism by synthetic REV-ERB agonists. Nature 2012;485(7396):62–8 doi 10.1038/nature11030. [PubMed: 22460951]
38. Hirota T, Lee JW, St John PC, Sawa M, Iwaisako K, Noguchi T, et al. Identification of small molecule activators of cryptochrome. Science 2012;337(6098):1094–7 doi 10.1126/science.1223710. [PubMed: 22798407]
39. Lamia KA, Papp SJ, Yu RT, Barish GD, Uhlenhaut NH, Jonker JW, et al. Cryptochromes mediate rhythmic repression of the glucocorticoid receptor. Nature 2011;480(7378):552–6 doi 10.1038/nature10700. [PubMed: 22170608]
40. Narasimamurthy R, Hatori M, Nayak SK, Liu F, Panda S, Verma IM. Circadian clock protein cryptochrome regulates the expression of proinflammatory cytokines. Proceedings of the National Academy of Sciences of the United States of America 2012;109(31):12662–7 doi 10.1073/pnas.1209965109. [PubMed: 22778400]
41. Humphries PS, Bersot R, Kincaid J, Mabery E, McCluskie K, Park T, et al. Carbazole-containing amides and ureas: Discovery of cryptochrome modulators as antihyperglycemic agents. Bioorganic & medicinal chemistry letters 2018;28(3):293–7 doi 10.1016/j.bmcl.2017.12.051. [PubMed: 29292223]
42. Panda S, Antoch MP, Miller BH, Su AI, Schook AB, Straume M, et al. Coordinated transcription of key pathways in the mouse by the circadian clock. Cell 2002;109(3):307–20. [PubMed: 12015981]
43. Oshima T, Niwa Y, Kuwata K, Srivastava A, Hyoda T, Tsuchiya Y, et al. Cell-based screen identifies a new potent and highly selective CK2 inhibitor for modulation of circadian rhythms and cancer cell growth. Science Advances 2019;5(1):eaau9060 doi 10.1126/sciadv.aau9060. [PubMed: 30746467]
44. Levi F. Circadian chronotherapy for human cancers. Lancet Oncol 2001;2(5):307–15 doi 10.1016/S1470-2045(00)00326-0. [PubMed: 11905786]
45. Perelis M, Marcheva B, Ramsey KM, Schipma MJ, Hutchison AL, Taguchi A, et al. Pancreatic beta cell enhancers regulate rhythmic transcription of genes controlling insulin secretion. Science 2015;350(6261):aac4250 doi 10.1126/science.aac4250. [PubMed: 26542580]
46. Hofman EG, Ruonala MO, Bader AN, van den Heuvel D, Voortman J, Roovers RC, et al. EGF induces coalescence of different lipid rafts. Journal of cell science 2008;121(Pt 15):2519–28 doi 10.1242/jcs.028753. [PubMed: 18628305]
47. Le A, Cooper CR, Gouw AM, Dinavahi R, Maitra A, Deck LM, et al. Inhibition of lactate dehydrogenase A induces oxidative stress and inhibits tumor progression. Proceedings of the National Academy of Sciences of the United States of America 2010;107(5):2037–42 doi 10.1073/pnas.0914433107. [PubMed: 20133848]

48. Patra KC, Wang Q, Bhaskar PT, Miller L, Wang Z, Wheaton W, et al. Hexokinase 2 is required for tumor initiation and maintenance and its systemic deletion is therapeutic in mouse models of cancer. Cancer cell 2013;24(2):213–28 doi 10.1016/j.ccr.2013.06.014. [PubMed: 23911236]

49. Flavahan WA, Wu Q, Hitomi M, Rahim N, Kim Y, Sloan AE, et al. Brain tumor initiating cells adapt to restricted nutrition through preferential glucose uptake. Nature neuroscience 2013;16(10): 1373–82 doi 10.1038/nn.3510. [PubMed: 23995067]

50. Ciccarone F, Vegliante R, Di Leo L, Ciriolo MR. The TCA cycle as a bridge between oncometabolism and DNA transactions in cancer. Seminars in cancer biology 2017;47:50–6 doi 10.1016/j.semcancer.2017.06.008. [PubMed: 28645607]

51. Shim EH, Livi CB, Rakheja D, Tan J, Benson D, Parekh V, et al. L-2-Hydroxyglutarate: an epigenetic modifier and putative oncometabolite in renal cancer. Cancer discovery 2014;4(11): 1290–8 doi 10.1158/2159-8290.CD-13-0696. [PubMed: 25182153]

52. Dierickx P, Emmett MJ, Jiang C, Uehara K, Liu M, Adlanmerini M, et al. SR9009 has REV-ERB-independent effects on cell proliferation and metabolism. Proceedings of the National Academy of Sciences of the United States of America 2019;116(25):12147–52 doi 10.1073/pnas.1904226116. [PubMed: 31127047]

53. Nangle S, Xing W, Zheng N. Crystal structure of mammalian cryptochrome in complex with a small molecule competitor of its ubiquitin ligase. Cell research 2013;23(12):1417–9 doi 10.1038/cr.2013.136. [PubMed: 24080726]

54. Kondratov RV, Kondratova AA, Gorbacheva VY, Vykhovanets OV, Antoch MP. Early aging and age-related pathologies in mice deficient in BMAL1, the core componentof the circadian clock. Genes & development 2006;20(14):1868–73 doi 10.1101/gad.1432206. [PubMed: 16847346]

55. Filbin M, Monje M. Developmental origins and emerging therapeutic opportunities for childhood cancer. Nature Medicine 2019;25(3):367–76 doi 10.1038/s41591-019-0383-9.

56. Bao S, Wu Q, McLendon RE, Hao Y, Shi Q, Hjelmeland AB, et al. Glioma stem cells promote radioresistance by preferential activation of the DNA damage response. Nature 2006;444(7120): 756–60 doi 10.1038/nature05236. [PubMed: 17051156]

STATEMENT OF SIGNIFICANCE

Cancer stem cells are highly malignant tumor populations. We demonstrate that glioblastoma stem cells selectively depend on circadian regulators with gained binding sites promoting tumor metabolism accompanied with active chromatin regions. Supporting clinical relevance, pharmacologic targeting of circadian networks specifically disrupted cancer stem cell growth and self-renewal.

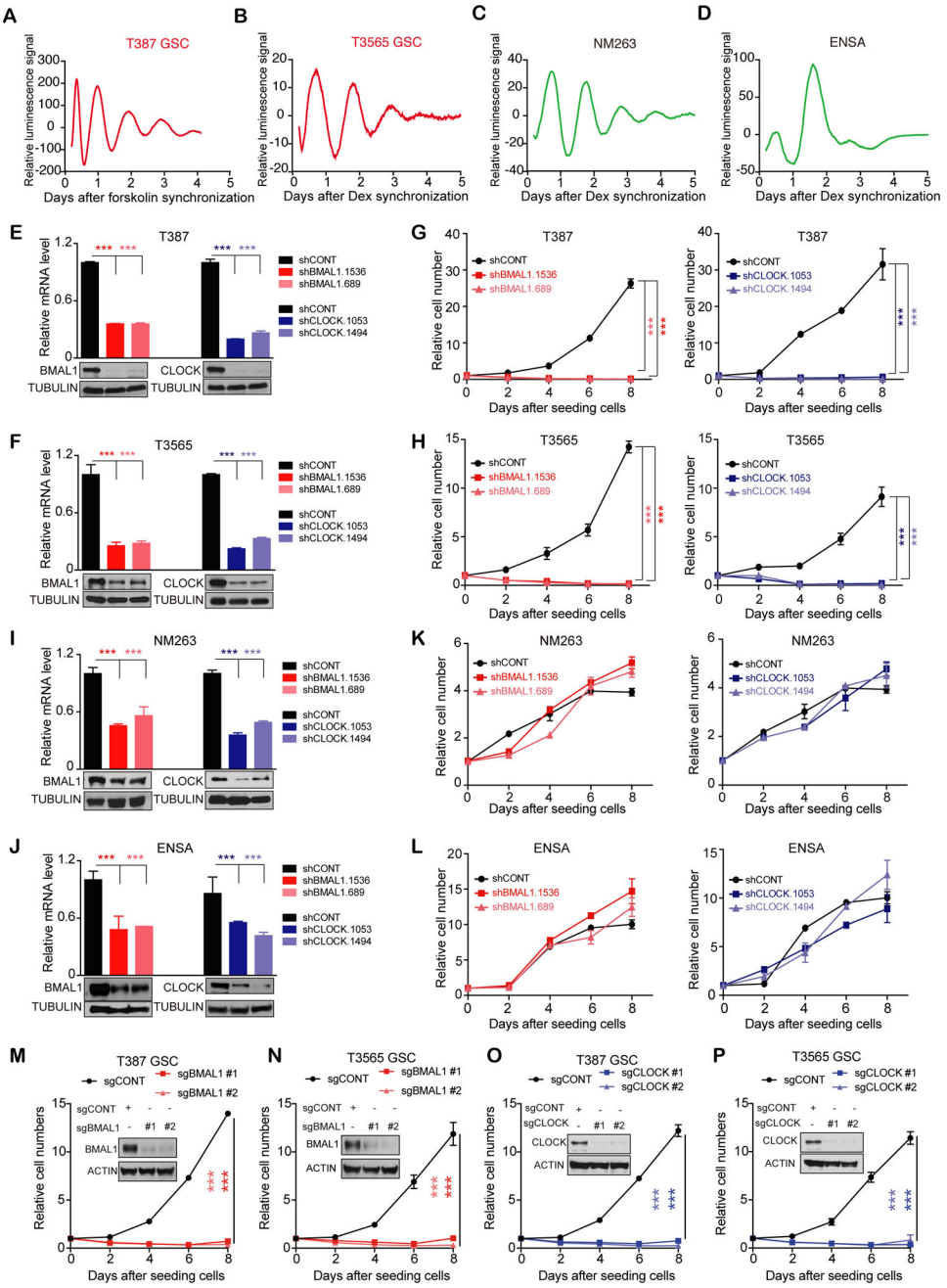

Figure 1. Genetic disruption of core clock genes suppresses GSC growth despite robust circadian oscillation.

(**A-D**) Bioluminescence of BMAL1::Luc in T387 (A) and T3565 (B) GSCs, non-malignant brain cultures (C), NSC (ENSA) (D), synchronized by 100 nM dexamethasone or 10 μM forskolin. Data are representative of three experiments.

(**E** and **F**) mRNA and protein expression of BMAL1 and CLOCK in T387 (E) and T3565 (F) GSCs transduced with shCONT, shBMAL1 or shCLOCK. Data are presented as mean ± SD. ***, P< 0.001. Statistical significance was determined by one-way ANOVA with Tukey's multiple comparison. N=3.

(**G** and **H**) Relative cell numbers of T387 (G) and T3565 (H) GSCs transduced with shCONT, shBMAL1 or shCLOCK. Data are presented as mean ± SD. ***, P< 0.001. Statistical significance was determined by two-way ANOVA with Tukey's multiple comparison. N=4.

(**I** and **J**) mRNA and protein expression of BMAL1 and CLOCK in non-malignant brain cultures (NM 263) (I) and NSC (ENSA) (J) transduced with shCONT, shBMAL1 or shCLOCK. Data are presented as mean ± SD. ***, P< 0.001. Statistical significance was determined by one-way ANOVA with Tukey's multiple comparison. N=3.

(**K** and **L**) Relative cell numbers of non-malignant brain cultures (K) and NSCs (L) transduced with shCONT, shBMAL1 or shCLOCK. Data are presented as mean ± SD. ***, P< 0.001. Statistical significance was determined by two-way ANOVA with Tukey's multiple comparison. N=4.

(**M**-**P**) Protein expression of BMAL1 or CLOCK and relative cellular numbers in GSCs transduced with Cas9-sgCONT, Cas9-sgBMAL1 (M and N) or Cas9-sgCLOCK (O and P). Data are presented as mean ± SD. ***, P< 0.001. Statistical significance was determined by two-way ANOVA with Tukey's multiple comparison. N=3.

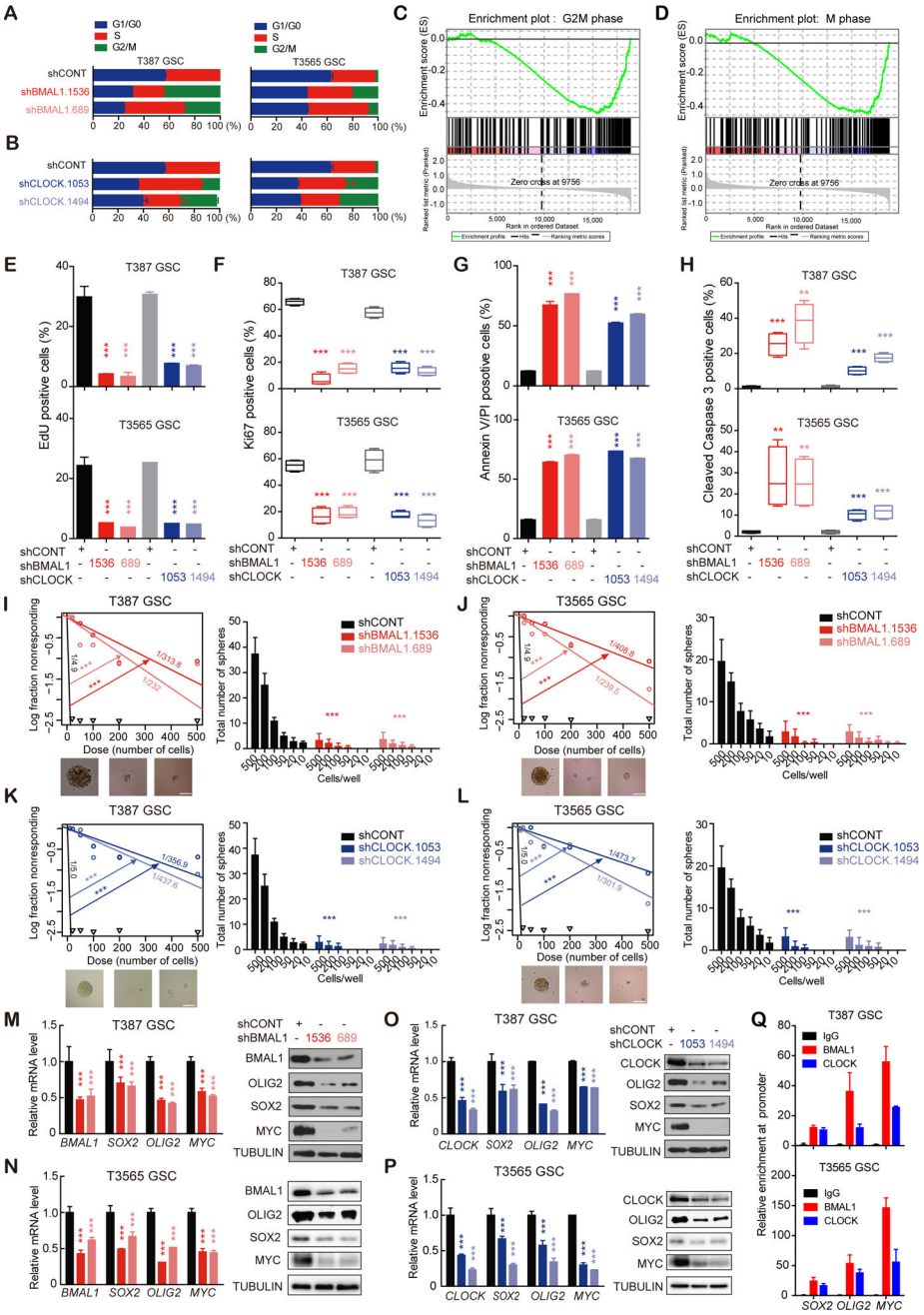

Figure 2. The core clock components, BMAL1 and CLOCK, are indispensable for GSCs proliferation and survival.

(**A** and **B**) Cell cycle analysis of GSCs following transduction with shCONT, sh*BMAL1* (A) or sh*CLOCK* (B). N=3.

(**C** and **D**) GSEA plot of genes in G2M (C) and M phase (D) during cell cycle after *BMAL1* knockdown in GSCs.

(**E**) Quantification of EdU incorporation in GSCs transduced with shCONT, sh*BMAL1* or sh*CLOCK*. Data are presented as mean ± SD. ***, $P<0.001$. Statistical significance was determined by one-way ANOVA with Tukey's multiple comparison. N=3.

(**F**) Quantification of Ki67-positive cells by immunofluorescent staining in GSCs after transduction with shCONT, sh*BMAL1* or sh*CLOCK*. Data are presented as mean ± SD. ****, P*< 0.001. Statistical significance was determined by one-way ANOVA with Tukey's multiple comparison. N=4.

(**G**) Quantification of FITC-Annexin V/PI positive cells of GSCs transduced with shCONT, sh*BMAL1* or sh*CLOCK*. Data are presented as mean ± SD. ****, P*< 0.001. Statistical significance was determined by one-way ANOVA with Tukey's multiple comparison. N=3.

(**H**) Quantification of cleaved CASPASE3 positive cells by immunofluorescent staining in GSCs after transduction with shCONT, sh*BMAL1* or sh*CLOCK*. Data are presented as mean ± SD. ****, P*< 0.001. Statistical significance was determined by one-way ANOVA with Tukey's multiple comparison. N=4.

(**I**-**L**) In vitro limiting dilution assays and sphere formation of GSCs transduced with shCONT, sh*BMAL1* (I and J), or sh*CLOCK* (K and L). The estimated stem cell frequencies were indicated. Scale bar is 100 μm. Data of sphere numbers are presented as mean ± SD. ****, P*< 0.001. Statistical significance of sphere numbers was determined by one-way ANOVA with Tukey's multiple comparison. $\chi 2$ test was used for pair-wise differences in stem population frequency. N=3.

(**M**-**P**) Transcripts and protein levels of GSC regulatory factors (*SOX2, OLIG2* and *MYC*) measured by quantitative PCR and immunoblot in GSCs transduced with shCONT, sh*BMAL1* (M and N), or sh*CLOCK* (O and P). Data are presented as mean ± SD. ****, P*< 0.001. Statistical significance was determined by two-way ANOVA with Tukey's multiple comparison. N=3.

(**Q**) ChIP-qPCR experiments showing occupancy of BMAL1 at the promoters of *SOX2*, *OLIG2* and *MYC*. All the results are normalized to IgG control. N=3.

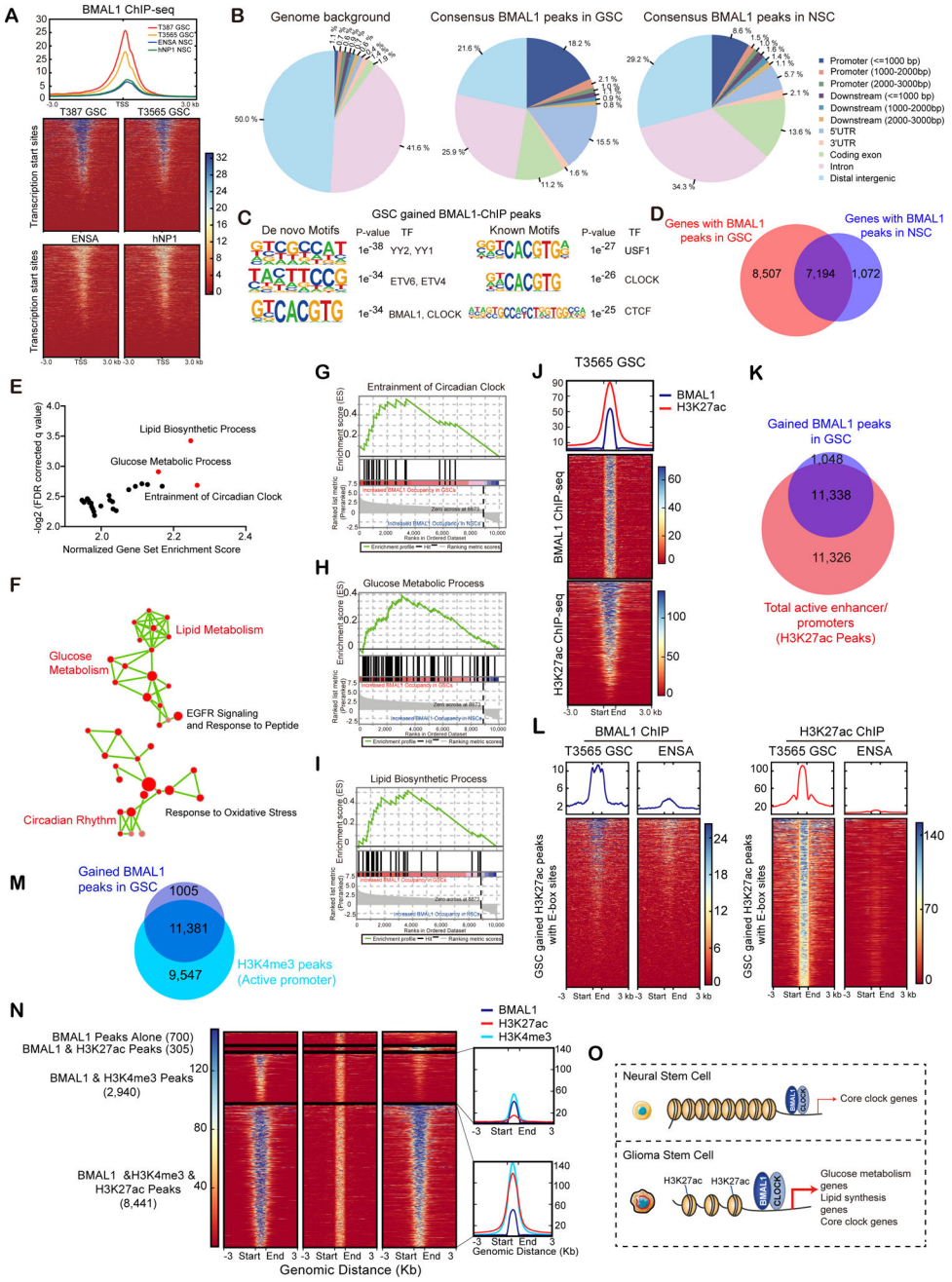

Figure 3. BMAL1 exhibits aberrant genome-wide binding patterns in GSCs compared to NSCs.

(**A**) Binding profiles and heatmaps for BMAL1 ChIP-seq signals in GSCs (T387 and T3565) and NSCs (ENSA and hNP1). ChIP-seq signals are displayed within a region spanning ±3 kb around all canonical transcription start sites (TSS) genome-wide.

(**B**) Distribution of genomic annotations of BMAL1 peaks in GSCs (middle panel) and NSCs (right panel) with background shown in left panel. Consensus peaks were derived by selecting all peaks present in both replicates of respective cell types.

(**C**) Motif analysis of GSC-gained BMAL1 binding sites as defined in (Figure S4C). Both de novo (left) and known consensus (right) motifs are shown with corresponding enrichment significance values.

(**D**) Venn diagram showing the overlap between BMAL1 binding genes in GSCs and NSCs ±3 kb around the TSS.

(**E** and **F**) Gene set enrichment analysis (GSEA) (E) and pathway enrichment bubble plots (F) of genes with GSC-gained BMAL1 peaks ±3 kb around the TSS.

(**G-I**) GSEA plots of genes involved in circadian rhythm (G), glucose regulation (H) and lipid metabolism (I) with increased BMAL1 binding in GSCs relative to NSCs.

(**J**) Heatmaps showing correlation of BMAL1 and H3K27ac ChIP-seq in T3565 GSCs. All ChIP-seq signals are displayed from ±3 kb surrounding each annotated BMAL1 peak.

(**K**) Venn diagram showing the overlap between gained BMAL1 and H3K27ac peaks in T3565 GSCs.

(**L**) Heatmaps displaying BMAL1 and H3K27ac ChIP-seq signals across GSC-gained H3K27ac peaks containing an E-box motif.

(**M**) Venn diagram showing the overlap between GSC-gained BMAL1 peaks and H3K4me3 peaks in GSCs.

(**N**) Heatmaps showing correlation of BMAL1, H3K4me3 and H3K27ac ChIP-seq in GSCs.

(**O**) Schematic showing differential BMAL1 chromatin binding in NSCs and GSCs.

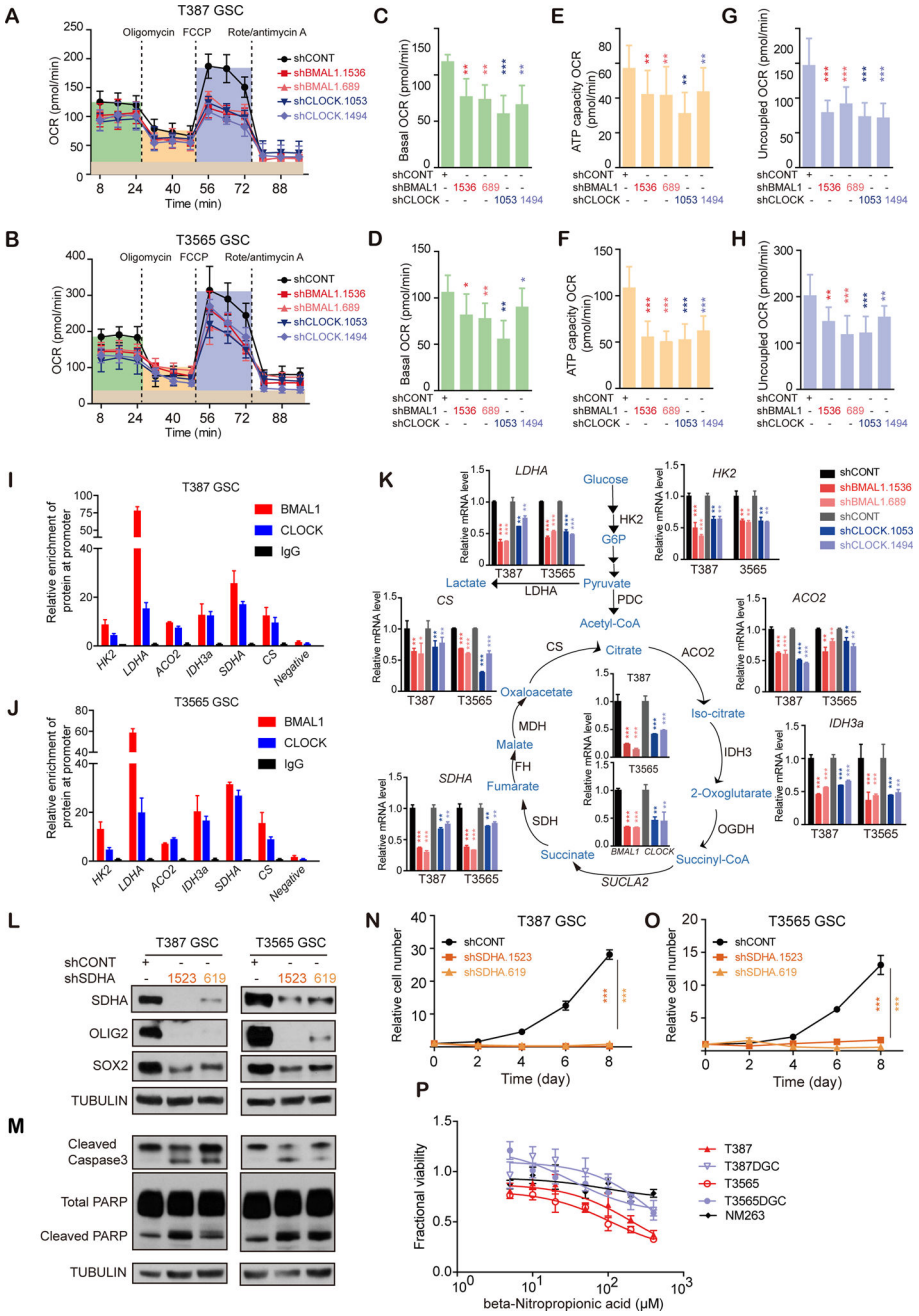

Figure 4. Core clock components contribute to oxidative phosphorylation and TCA cycle in GSCs.

(**A** and **B**) Oxidative phosphorylation (OXPHOS) of T387 (A) and T3565 (B) GSCs after transduction with shCONT, sh*BMAL1* or sh*CLOCK* using seahorse extracellular flux analyzer (XF) OCR indicates OXPHOS. Cells were sequentially treated as indicated with oligomycin (2 μM), P-trifluoromethoxy carbonyl cyanide phenylhydrazone (FCCP, 2 μM), antimycin A (1 μM) and rotenone (rote, 1 μM). Vertical line indicates the time points for inhibitors administration. Data are presented as mean ± SEM. N=3.

(**C** and **D**) Histograms of basal oxidative phosphorylation in T387 (C) and T3565 (D) GSCs transduced with shCONT, sh*BMAL1* or sh*CLOCK*. Data are presented as mean ± SEM. **,*

P< 0.05; ***, *P*< 0.01; ****, *P*< 0.001. Statistical significance was determined by one-way ANOVA with Tukey's multiple comparison. N=3.

(**E** and **F**) ATP capacity of T387 (E) and T3565 (F) GSCs transduced with shCONT, sh*BMAL1* or sh*CLOCK*. Data are presented as mean ± SEM. ***, *P*< 0.01; ****, *P*< 0.001. Statistical significance was determined by one-way ANOVA with Tukey's multiple comparison. N=3.

(**G** and **H**) Levels of uncoupled OXPHOS in T387 (G) and T3565 (H) GSCs transduced with shCONT, sh*BMAL1* or sh*CLOCK*. Data are presented as mean ± SEM. ***, *P*< 0.01; ****, *P*< 0.001. Statistical significance was determined by one-way ANOVA with Tukey's multiple comparison. N=3.

(**I** and **J**) ChIP-qPCR experiments showing BMAL1 and CLOCK occupancy at the promoter region of the indicated genes in T387 (I) and T3565 (J) GSCs. All the results are normalized to IgG control. N=3.

(**K**) Transcript levels of the indicated genes related to glycolysis and tricarboxylic acid cycle in GSC upon *BMAL1* or *CLOCK* knockdown. Data are presented as mean ± SD. *, *P*< 0.05; ***, *P*< 0.01; ****, *P*< 0.001. Statistical significance was determined by one-way ANOVA with Tukey's multiple comparison. N=3.

(**L**) Protein levels of critical GSC transcription factors (*SOX2* and *OLIG2*) after targeting *SDHA* with shRNAs for 48 hours. N=3.

(**M**) Immunoblotting of cleaved CASPASE 3 and cleaved PARP in GSCs transduced with shCONT or sh*SDHA*. N=3.

(**N** and **O**) Cell survival analysis of T387 (N) and T3565 (O) GSCs transduced with shCONT or sh*SDHA*. Relative cell survival was measured at indicated day (0, 2, 4, 6, or 8). Data are presented as mean ± SD. ****, *P*< 0.001. Statistical significance was determined by two-way ANOVA with Tukey's multiple comparison. N=3.

(**P**) Concentration-responsive curve of GSCs (T387 GSC and T3565 GSC), DGCs (T387 DGC and T3565 DGC) and non-malignant brain cultures (NM263) treated with beta-Nitropropionic acid (NPA) for 3 days. N = 3.

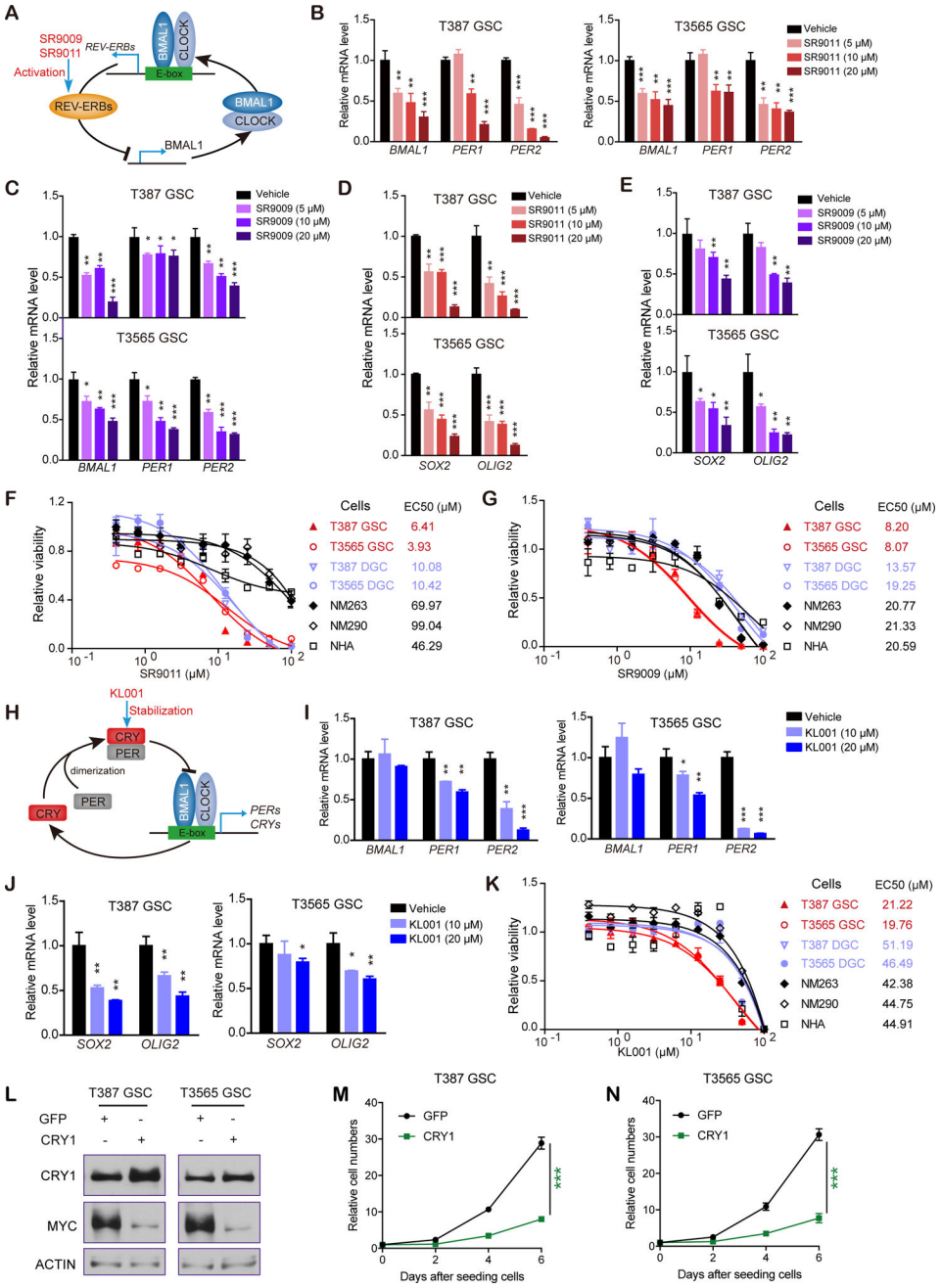

Figure 5. Targeting BMAL1 with small molecules provides a therapeutic strategy for glioma.

(**A**) Schematic of negative feedback loop driven by REV-ERBs and BMAL1::CLOCK. Small molecules SR9011 and SR9009 repress *BMAL1* expression by activating REV-ERBs. (**B** and **C**) Transcript levels of core clock genes measured by quantitative RT-PCR in two GSCs treated with different concentrations of SR9011 (B) or SR9009 (C) for 3 days. Data are presented as mean ± SD. *, $P< 0.05$; **, $P< 0.01$; ***, $P< 0.001$. Statistical significance was determined by two-way ANOVA with Tukey's multiple comparison. N=3. (**D** and **E**) Transcript level of GSC markers in two GSCs incubated with different concentrations of SR9011 (D) or SR9009 (E) for 3 days in vitro. N=3. *, $P< 0.05$; **, $P<$

0.01; ****, P*< 0.001. Statistical significance was determined by two-way ANOVA with Tukey's multiple comparison. N=3.

(**F** and **G**) Concentration-response curves and EC50 of various cell types treated with SR9011 (F) or SR9009 (G) (x axis, log scale). T387 and T3565 are GSCs, T387 DGC and T3565 DGC are DGCs, NM263 and NM290 are non-malignant brain cultures, NHA is astrocyte. N=3. Data are presented as mean ± SD.

(**H**) Schematic of CRYs feedback loop. The small molecule modulator KL001 inhibits BMAL1 activity via stabilizing CRY1.

(**I** and **J**) Transcript expression of core clock genes (I) and GSC markers (J) measured by quantitative RT-PCR following treatment of GSCs with different concentrations of KL001 for 3 days. Data are presented as mean ± SD. **, P*< 0.05; ***, P*< 0.01; ****, P*< 0.001. Statistical significance was determined by two-way ANOVA with Tukey's multiple comparison. N=3.

(**K**) Concentration-response curves and EC50 of GSCs (T387 and T3565), DGCs (T387DGC and T3565DGC), non-malignant brain cultures (NM263 and NM290) and astrocytes (NHA) treated with different concentrations of KL001 (x axis, log scale) for 3 days. N=3.

(**L**) Immunoblot of CRY1 and MYC in GSCs overexpressing CRY1. Data are representative results from three-independent experiments.

(**M** and **N**) Relative cell numbers of GSCs overexpressing CRY1 or GFP. Data are presented as mean ± SD. ****, P*< 0.001. Statistical significance was determined by one-way ANOVA with Tukey's multiple comparison. N=3

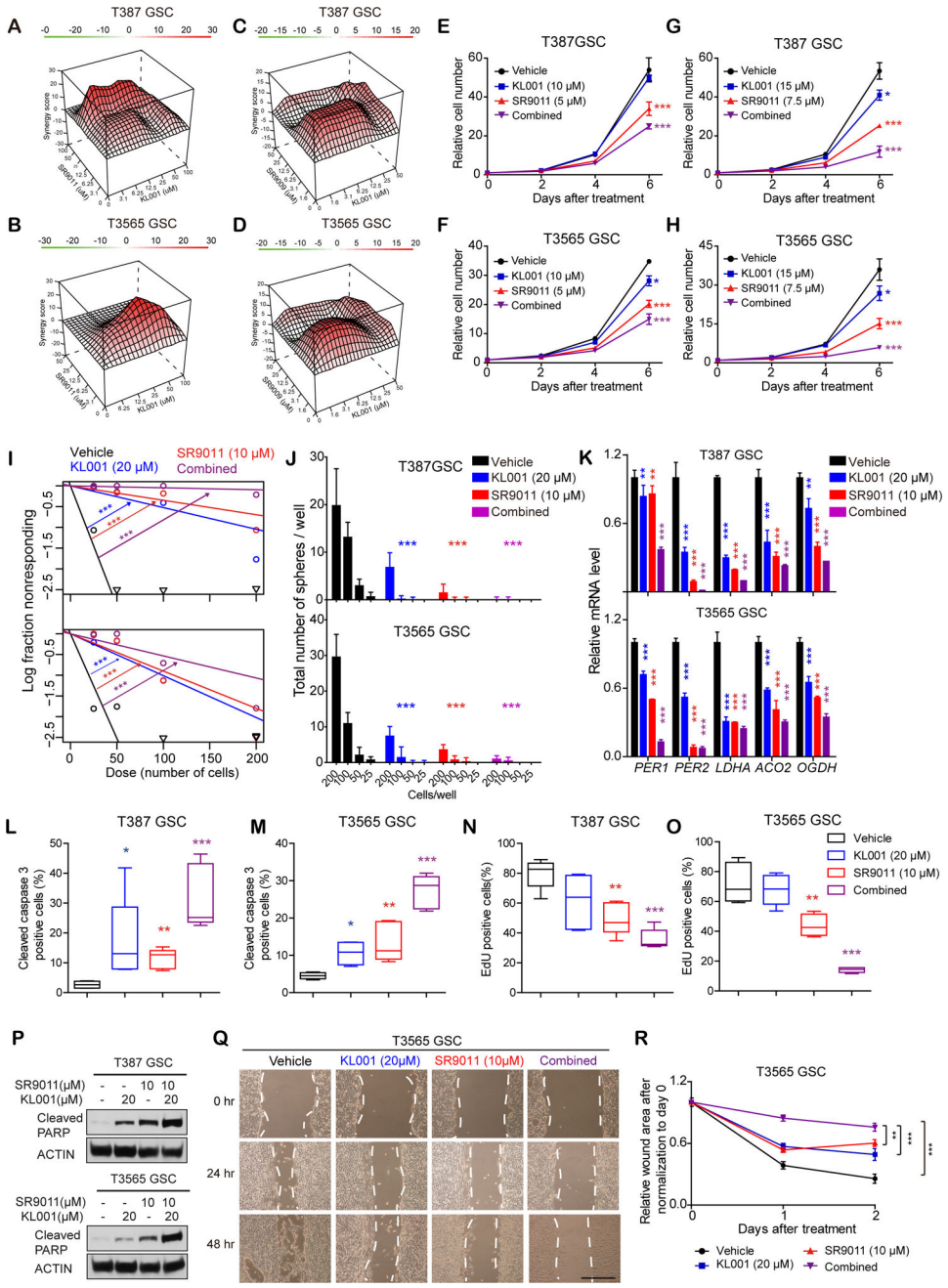

Figure 6. Synergism of REV-ERB and CRY agonists *in vitro*.

(**A-D**) Synergy indices of SR9011 and KL001 (A and B), SR9009 and KL001 (C and D) analyzed by R package “synergyfinder”.

(**E** and **F**) Relative cell survival of T387 (E) and T3565 (F) GSCs following treatment with indicated concentration of KL001 (10 μM), SR9011 (5 μM), or a combination. Data are presented as mean ± SD. **, P*< 0.05; ****, P*< 0.001. Statistical significance was determined by two-way ANOVA with Tukey’s multiple comparison. N=3.

(**G** and **H**) Relative cell viability of T387 (G) and T3565 (H) GSCs following treatment with indicated concentration of KL001 (15 μM), SR9011 (7.5 μM), or a combination. Data are

presented as mean ± SD. *, $P < 0.05$; ***, $P < 0.001$. Statistical significance was determined by one-way ANOVA with Tukey's multiple comparison. N=3.

(**I** and **J**) In vitro limiting dilution assays (I) and sphere numbers of GSCs (J) following treatment with KL001 and SR9011 at indicated concentrations for 8 days. Data of sphere numbers are presented as mean ± SD. ***, $P < 0.001$. Statistical significance of sphere numbers was determined by one-way ANOVA with Tukey's multiple comparison. $\chi 2$ test was used for pair-wise differences in stem population frequency. N=3.

(**K**) Relative mRNA level of circadian and metabolic genes after treatment with KL001 (20 μM), SR9011 (10 μM) or a combination. Data are presented as mean ± SD. *, $P < 0.05$; **, $P < 0.01$; ***, $P < 0.001$. Statistical significance was determined by two-way ANOVA with Tukey's multiple comparison. N=3.

(**L** and **M**) Quantification of cleaved CASPASE3 positive cells by immunofluorescent staining in T387 (L) and T3565 (M) GSCs after treatment with indicated agonists. Data are presented as mean ± SD. *, $P < 0.05$, **, $P < 0.01$, ***, $P < 0.001$. Statistical significance was determined by one-way ANOVA with Tukey's multiple comparison. N=3.

(**N** and **O**) Quantification of EdU positive cells by immunofluorescent staining in T387 (N) and T3565 (O) GSCs after treatment with indicated agonists for 48 hours. Data are presented as mean ± SD. **, $P < 0.01$, ***, $P < 0.001$. Statistical significance was determined by one-way ANOVA with Tukey's multiple comparison. N=3.

(**P**) Immunoblot of cleaved-PARP in GSCs after treatment with indicated agonists for 48 hours. Data are representative results of three independent experiments.

(**Q** and **R**) *In vitro* wound healing assay (Q) and calculated relative wound area (R) of T3565 GSCs treatment with indicated agonists. The scale bar is 0.4 mm. N=6. Data are presented as mean ± SD. **, $P < 0.01$; ***, $P < 0.001$. Statistical significance was determined by two-way ANOVA with Tukey's multiple comparison.

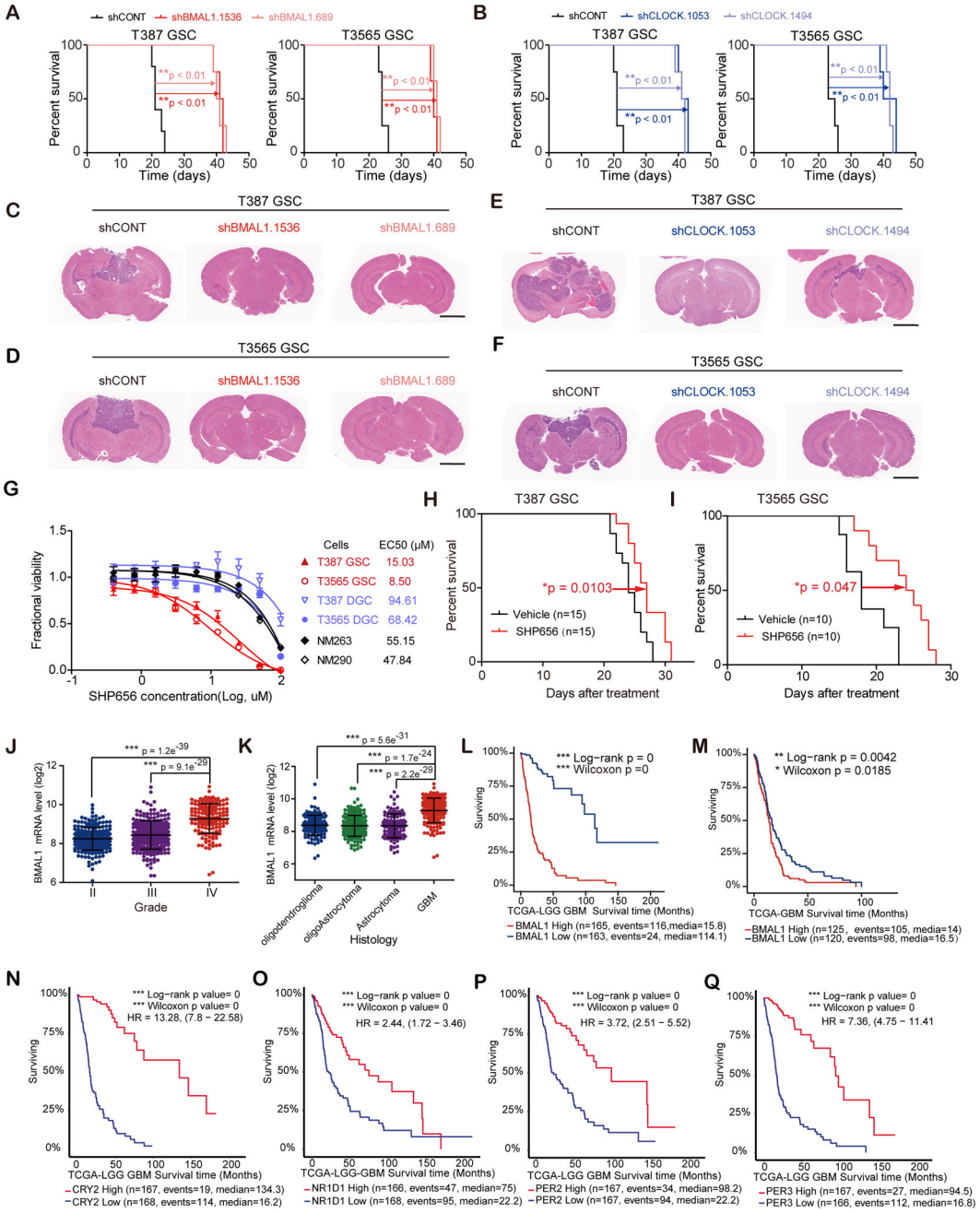

Figure 7. Targeting core clock components suppresses in vivo tumor growth.

(**A** and **B**) Kaplan-Meier survival curves of immunocompromised mice bearing GSCs transduced with shCONT (N = 5), sh*BMAL1* (N = 4) (A) or sh*CLOCK* (N = 4) (B). Statistical significance was determined by Mantel-Cox log-rank test.

(**C**-**F**) H&E staining of tumor-bearing brains following implantation of GSCs transduced with either shCONT, sh*BMAL1* (C and D) or sh*CLOCK* (E and F). Scale bar is 2 mm.

(**G**) Concentration-response curves and EC50 of GSCs (T387 and T3565), DGCs (T387DGC and T3565DGC), non-malignant brain cultures (NM263 and NM290) and

astrocytes (NHA) treated with different concentrations of SHP656 (x axis, log scale) for 3 days. N=3.

(**H** and **I**) Kaplan-Meier survival curves of mice bearing T387 GSC (H) or T3565 GSC (I) treated with SHP656. 15 mice were used per arm for T387 GSC and mice were treated BID (twice a day) at 10mg/Kg. 10 mice were used per arm for T3565 GSC and mice were treated QD (once a day) at 10mg/Kg. Statistical significance was determined by Mantel-Cox log-rank test.

(**J** and **K**) *BMAL1* mRNA level in different grades (J) or histologies (K) of glioma patients from TCGA dataset. Data are presented as mean ± SD. Statistical significance of sphere numbers was determined by one-way ANOVA with Tukey's multiple comparison.

(**L** and **M**) Kaplan-Meier survival curves of patients with higher or lower *BMAL1* expression in low grades of glioma and glioblastoma (L) or glioblastoma alone (N). Statistical significance was determined by Mantel-Cox log-rank test.

(**N-Q**) Kaplan-Meier survival curves of patients with higher or lower *CRY2* (N), *NR1D1* (O), *PER2* (P) *or PER3* (Q) expression in low grades of glioma and glioblastoma. Statistical significance was determined by Mantel-Cox log-rank test.